Review

Helical Actuators Inspired by Chiral Seedpod Opening and Tendril Coiling

Guangchao Wan †, Congran Jin †, Ian Trase, Shan Zhao and Zi Chen *

Thayer School of Engineering, Dartmouth College, Hanover, New Hampshire, 03755, USA;
guangchao.wan.th@dartmouth.edu (G.W.); congran.jin.th@dartmouth.edu (C.J.);
ian.trase.th@dartmouth.edu (I.T.); shan.zhao@dartmouth.edu (S.Z.); zi.chen@dartmouth.edu (Z.C.)
* Correspondence: zi.chen@dartmouth.edu; Tel.: +1-603-646-6475

† These authors contribute equally to this work

Abstract: Actuators are essential components for intelligent machines that can fulfill certain tasks in response to environmental stimuli. In recent years, actuators that can transform from a 2D ribbon shape to a 3D helical configuration under certain external stimuli have attracted significant attention due to the potential applications of the targeted helical structures in springs, propulsion generation, and artificial muscles. Inspired by the chiral opening of *Bauhinia variegate*'s seedpods and the coiling of the *Towel Gourd* tendril with perversions, researchers have made significant breakthroughs in synthesizing state-of-the-art actuators capable of mimicking helical transformations. In this review, we give a brief overview of the shape evolution mechanisms of these two plant structures and then review recent progress in the fabrication of biomimetic helical actuators. These structures are categorized by the stimuli-responsive materials involved, including hydrogels, liquid crystal networks/elastomers, shape memory polymers, and multiwall carbon nanotubes. By providing this survey on important recent advances along with our perspectives, we hope to solicit new inspirations and insights on the development and fabrication of smart actuators, as well as the future development of interdisciplinary research at the interface of physics, engineering, and biology.

Keywords: bioinspired; seedpod opening; tendril coiling; helical actuators; stimuli-responsive materials

1. Introduction

Advanced actuators can deform in response to external stimuli such as heat, light, PH or pneumatic pressure, making them excellent components in intelligent machines. Deformations include planar expansion/contraction, bending, twisting, and complex motions that are in high demand in applications such as soft robotics [1], metamaterials [2] and self-morphing structures [3]. Among these various actuation modes, helical actuation, in which a 2D flat sheet deforms into a 3D helix and then winds or unwinds itself to provide contraction or rotary motion under external stimuli, has been attracting intense attention from applied mathematicians, physicists, and engineers alike. The research motivation comes from two aspects. The first stems from the significant role of helical shapes in both biological processes such as the seed's penetration in soil [4] or the motion of E. *coil* in body fluids [5] and in engineering applications including the propulsion of a swimming micro-robot [6] or stretchable electronic devices [7]. The second motivation is that direct fabrication of a 3D helix is difficult while 2D patterning has become easier as photo-lithography develops. It is therefore important to determine how to make 2D to 3D helical actuation easier and more programmable, for example, building upon the pioneering work on bi-layer beam bending by Timoshenko [8].

Nature teems with excellent examples of this type of shape transition. During the opening process of the *Bauhinia variegate* pod, an initially flat pod valve changes into a helix through a hydroscopic process [9]. *Towel Gourd* tendrils similarly coil while growing [10]. For the seedpod

opening, the underlying mechanism originates from the oriented cellulose fiber distribution inside the matrix [9]. The fiber reinforcement restricts the swelling/deswelling deformation of the organic matrix along the fiber's direction without much impact on the deformation perpendicular to the reinforcement direction. As a result, anisotropic deformation of plant's matrix leads to mechanical frustration which can only be resolved by transitioning the planar shape into a 3D helical configuration. For the coiling of *Towel Gourd* tendril, a hierarchical chirality which spans several length scales was discovered interpret the transfer of the individual cells' chirality into macroscopic tendril coiling.

Inspired by the shape-shifting mechanism of *Bauhinia variegate*'s pod, researchers successfully synthesized various actuators by using stimuli-responsive materials such as hydrogels [11], liquid crystal networks/elastomers [12], and other functional materials. The radius and pitch of the targeted helix are determined by several parameters, including the geometry and swelling/deswelling ratios of different components. Another class of helical actuators is built to mimic the chirality transfer of *Towel Gourd* tendrils by assembling the chiral build blocks to fabricate an artificial helix [13]. In this example, the actuator is based on a two-level twisting of multiwall carbon nanotubes, which can wind or unwind when exposed to vapor or electrical signal, ideal for applications such as artificial muscles.

Here we provide a brief review on recent helical actuators that use similar actuation methods to *Bauhinia variegate*'s pod opening and *Towel Gourd* tendril's coiling. Our focus is to illustrate the shape-shifting mechanisms of these two plants and introduce stimuli-responsive materials which can be tailored to actuate in an equivalent manner. In section 2, helical actuators inspired from *Bauhinia variegate* are introduced according to their type of functional material, including hydrogels, liquid crystal networks/elastomers, and shape memory polymers. Each subsection is further organized based on the kind of responsive stimuli, such as thermal or light. In section 3, we concentrate on the coiling mechanism of *Towel Gourd* tendrils and present some biomimetic examples which exhibit the tendril's winding or unwinding behavior using carbon nanotubes. We close with an outlook on the potential opportunities and future challenges in this field.

2. Helical Actuators Inspired from the Opening of the *Bauhinia Variegate* Pod

2.1. Opening Mechanism of Bauhinia Variegate's Pod

2.1.1. Hydroscopic Motion in Plants

Plants can move in response to external stimuli such as a change in humidity or the approach of prey. Examples includes the snapping of the Venus flytrap (*Dionaea muscipla*) [14], the opening of pine cones [15], and the seed dispersal of wheat awns [16]. Different from muscle-actuated animal motion, plant motion results from water-driven swelling or shrinkage of cells inside the tissue [17]. During these hydroscopic processes, the swelling or shrinkage of the tissue will usually be guided by the microstructure of the cell wall where aligned cellulose fibrils are embedded. Resembling artificial fiber-reinforced composites, tissue deformation along the fiber alignment direction will be restricted while shape change perpendicular to the fiber orientation will be less affected. This anisotropic deformation contributes to the sophisticated motion of plants.

One well-known example of humidity-driven plant actuation is the opening process of the *Bauhinia variegate* pod valve (Figure 1a), the underlying mechanism of which is illustrated in [9]. The microstructure of this seedpod consists of two fibrous layers. The fiber's orientation in one layer is perpendicular to the other, and both have a 45° angle relative to the long axis of the seedpod. When the air is dry, the cells in the sclerenchyma tissue will lose water and make the tissue matrix shrink. Owing to the cellulose fiber reinforcement, shrinkage only occurs perpendicular to the fiber's orientation in each layer, and the two layers in the seedpod valve shrink perpendicular to each other. As a result, the thin pod valve prefers to adopt a saddle shape by bending into opposite curvatures along two orthogonal directions, which can be proven by the mechanical analog in which two

uniaxially stretched elastomer sheets are attached together (Figure 1b). This saddle shape will drive the flat pod into a helix, which can be predicted using the non-Euclidean theory.

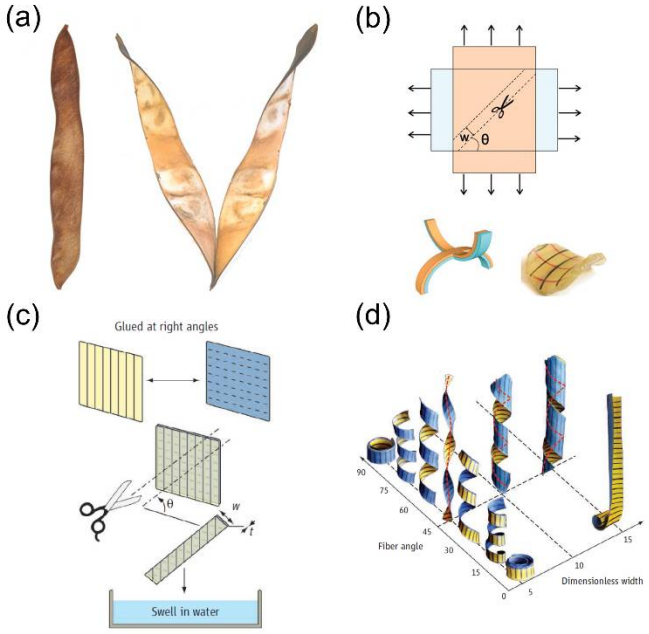

Figure 1. The opening mechanism of the *Bauhinia variegate* pod. (**a**) A closed seedpod in a wet environment (left) and the opened seedpod in a dry environment (right); (**b**) Mechanical analog of seedpod opening by attaching two uniaxially stretched elastomer sheets together and cutting a ribbon at an angle θ with width w (top). The bilayer sheet adopts a saddle shape: illustrated (bottom left), experimental (bottom right); (**c**) The process to generate helices using a bilayer paper sheet reinforced with fibers; (**d**) Design space for helix generation with respect to the fiber angle and the non-dimensionalized width. (**a**) and (**b**) are from Ref. [9], reprinted from permission from AAAS; (**c**) and (**d**) are from Ref. [18], reprinted from permission from AAAS.

2.1.2. Transition from Pure Twisting to Helical Coiling During Pod Opening

A detailed derivation shows that the radius r and pitch p of the final helical seedpod are determined by several parameters including the intrinsic curvature κ_0, the angle between the fiber's orientation and seedpod's long axis θ, the seedpod thickness t, and the width w. The influence of these multiple parameters can be generalized into a dimensionless width $\tilde{w} = w\sqrt{\kappa_0/t}$, which reflects the relative magnitude of the bending energy and stretching energy [9,19]. Forterre et al. [18] provided an overview of the parametric study with respect to this dimensionless width $\tilde{w}$ and the fiber misoriented angle θ (Figure 1c). Fibers are aligned inside a paper sheet and two sheets are bonded with a tilting angle between the fiber reinforcement. A helix can be generated when the bilayer is swollen in water.

When $\tilde{w} \gg 1$, stretching is dominant. The Gaussian curvature $K = \kappa_1\kappa_2$ (κ_1 and κ_2 are the two principal curvatures) is zero everywhere to avoid planar stretching except at a boundary layer with a characteristic length scale $\sqrt{t/\kappa_0}$ [9,19,20]. The seedpod coils into a cylindrical helix along either of the two principal directions of the local saddle shape. When $\tilde{w} \ll 1$, the energy cost from bending is high while stretching is favorable. The Gaussian curvature K can be negative while the mean curvature $H = (\kappa_1 + \kappa_2)/2$ will be zero to minimize bending energy. The seedpod twists itself to accommodate the mechanical frustration while keeping the centerline straight. A transition from pure twisting to helical coiling as $\tilde{w}$ increases is not only observed in the pod valve, but is also demonstrated via a mechanical analog by attaching two stretched elastomer layers together in perpendicular directions [21]. Figure 1d quantitatively shows the impact of the fiber angle θ and dimensionless width $\tilde{w}$ on the helix shape. When $\theta = 45°$ and $\tilde{w}$ is small, the ribbon twists itself into a helicoid with a straight centerline. Deviation from this scenario will increase radius r and

decrease pitch p, which forms a spiral helical shape until it rolls up into a circular shape when $\theta = 90°$ or $0°$.

2.2. Actuators Inspired from Bauhinia Variegate's Pod

The mechanism of the chiral pod opening shows that a helix can be generated from any thin ribbon-like structure if a local saddle is created at an angle to the long axis of the ribbon. This mechanism is universal and can be realized, for example, by combining two layers with anisotropic pre-stretch in perpendicular directions [22] or using chiral molecules and building blocks in a single layer [23]. Such universality makes the *Bauhinia variegate* pod an outstanding prototype to inspire further fabrication of helical actuators.

The following sub-sections are organized based on the type of the functional material used in the helical actuator, among which are hydrogels, liquid crystal networks/elastomers, and shape memory polymers. We hope that this summary provides useful information for researchers from different fields for fabricating innovative bioinspired actuators.

2.2.1. Hydrogel-based Actuators

Hydrogels include a broad range of polymers and can be roughly defined as three-dimensional networks swollen by a solvent [24]. Compared to other stimuli-responsive materials, hydrogels can achieve reversible volume changes up to several folds when subjected to multiple stimuli such as humidity, temperature, ionic strength, or light. They provide an efficient pathway to realize large actuation via different controls. The open networks of hydrogels allow for subsequent chemical modification such as the formation of interpenetrating networks and for embedded additives such as stiff reinforcement or functional nanoparticles. This provides a variety of options to design actuators that can responding to different types of external signals. For further information, one can refer to Ref. [25].

Bulk hydrogels can only swell or deswell isotropically, which results in simple planar actuation. More complex shape transformation relies on the hybrid hydrogels in which the material composition varies either through the thickness [26] or along the planar directions [27–29]. Hu et al. [30] first reported the utilization of hydrogel to fabricate a bilayer beam which bends in response to mismatched strain between two layers. This pioneering work has inspired interest in hydrogel-based shape morphing structures. Recently, a similar idea was used to construct smart hinges which can fold or unfold microscale origami [31]. Utilizing an interpenetrating network formed through photo-crosslinking, Wu and co-workers [32] successfully fabricated a single-layer heterogeneous sheet with in-plane composition variation. The interaction between adjacent regions generates internal stress which buckles the planer sheet into various three-dimensional configurations such as helices, domes, or saddle shapes [33]. The authors harness material heterogeneity to enable a single sheet to respond to different stimuli, since each individual composition is sensitive to a specific stimulus. This greatly broadens the number of actuation modes available to a single hydrogel actuator [33,34].

In this sub-section, we describe hydrogel-based actuators which mimic the chiral opening of the *Bauhinia variegate* pod sorted by the type of stimulus: humidity, temperature, and pH. Embedded reinforcement guides the anisotropic swelling or deswelling of the hydrogel once actuated and creates an intrinsic saddle shape locally, leading to helical shape transformation.

2.2.1.1 Humidity-responsive Hydrogels

Water molecules can diffuse into or out of a hydrogel when humidity changes. When water is adsorbed, the space between polymer chains increases and the hydrogel swells. This shape change is isotropic, and its speed mainly depends on the rate of water diffusion.

Learning from nature, one could use fiber-like reinforcements to restrict deformation along the reinforced direction [35]. The isotropic swelling or deswelling of a hydrogel can thus be transformed into anisotropic deformation [36]. Zhang *et al.* [37] bury glass fibers inside agarose hydrogel as a reinforcement to guide the bending of a hydrogel ribbon when it is exposed to humidity on one side.

Peer-reviewed version available at Sensors 2018, 18, 2973; doi:10.3390/s18092973

Gladman *et al.* [11] mimic the seedpod microstructure by 3D-printing the cellulose fibrils inside the hydrogel matrix. By harnessing shear-induced alignment when the ink is ejected from the nozzle, the cellulose fibrils are aligned along the longitudinal direction of the printed filament and hence it is possible to locally control the fibril direction (Figure 2a). Once the hybrid hydrogel is swollen in solution, the transverse swelling ratio of the filament becomes larger than the longitudinal swelling ratio. This anisotropic swelling will yield a twisted helix when the filaments are aligned at ±45° relative to the long axis of the hydrogel ribbon (Figure 2b).

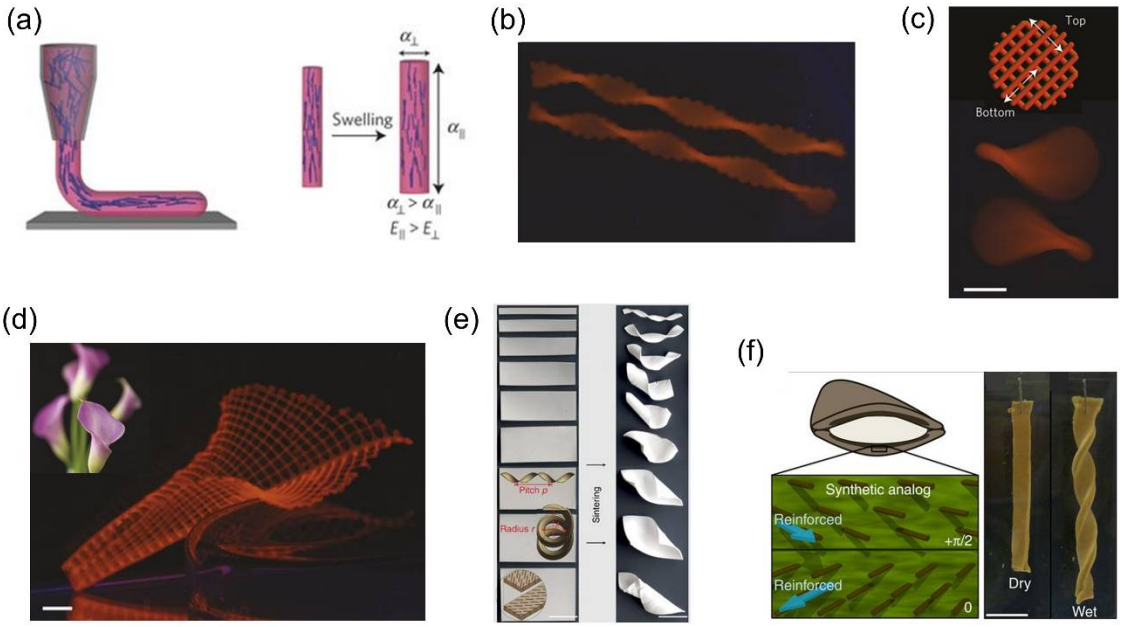

Figure 2. Humidity-responsive hydrogel-based helical actuators inspired from *Bauhinia variegate*. (**a**) Shear-induced alignment of cellulose fibrils along the printed filament (left) and anisotropic swelling of the printed filament (right); (**b**) Helical shape generated by 4D-printed hydrogel; (**c**) Saddle shape (bottom) from orthogonal patterns of filaments in two layers (top), the scale bar is 2.5mm; (**d**) Biomimetic lily flower from 4D-printed hydrogel, the inset is the lily flower in nature and the scale bar is 5mm; (**e**) Microplatelet-induced shape transformation from a planer sheet (left) to a helical shape (right) after sintering, the radius and pitch of the helix are influenced by the ribbon's width from top to bottom (right). The scale bar is 25mm; (**f**) Microplatelet alignment in a bilayer sheet (left) mimicking *Bauhinia variegate* and helical actuation of the synthesized hydrogel in water (right). The scale bar is 1cm. (a)-(d) are from Ref. [11], reproduced with permission, copyright 2016 Nature Publishing Group; (e) is from Ref. [38], reproduced with permission; (f) is from Ref. [39], reproduced with permission, copyright 2013 Nature Publishing Group.

The 3D-printing of stimuli-responsive materials that can programmably change shape is sometimes referred to as 4D printing. This technique gives one more tunable variable to the 3D printing, which makes it a powerful tool for designing stimuli-responsive structures [40].

The advantage of this biomimetic structure is that the 3D printing allows the filaments to be arranged horizontally in plane or vertically based on the printing path. A bilayer with orthogonal filaments will produce a saddle shape (Figure 2c). In-plane filaments allow for stretching while vertical filaments allow for bending. Accordingly, the Gaussian curvature *K*, which is related to the local stretching, and the mean curvature *H*, which depends on the bending, can be separately controlled. This offers the possibility to design any arbitrary surface on demand, such as a calla lily flower (Figure 2d).

The direction and distribution of the reinforcement can also be remotely controlled using magnetic [41,42] or electric fields [43]. Erb and collaborators [39] used ultra-low magnetic fields to guide the orientation of microplatelets (Al_2O_3) coated with superparamagnetic nanoparticles in a precursor solution. The orientation of the platelets was preserved during polymerization. By using

Preprints (www.preprints.org) | NOT PEER-REVIEWED | Posted: 5 July 2018 doi:10.20944/preprints201807.0094.v1

Peer-reviewed version available at Sensors 2018, 18, 2973; doi:10.3390/s18092973

two-step layer-by-layer fabrication and changing the magnetic field direction in each step, they obtain a bilayer hydrogel ribbon whose microstructure mimics the *Bauhinia variegate* pod. Like the seedpod, this hybrid hydrogel ribbon can either purely twist itself as a helicoid or coil into a spiral helix (Figure 2f) when exposed to external stimuli depending on the ribbon's width and reinforcement orientation during the fabrication process. This fabrication method puts no strict restriction on the matrix as the precursor solution does not severely retard the alignment of microplatelets during the curing process, which substantially broadens the scope of available materials and responsive stimuli. For example, such a mechanism can be realized via humidity-responsive gelatin, thermal-responsive hydrogel PNIPAM or even rigid ceramics [38] which shrink during the sintering process, and a similar transition from a helicoid to a spiral helix is also observed when the width increases (Figure 2e). This prototype can locally control the microplatelet orientation on demand, which makes it possible to program the target shape by spatially varying the reinforcement directions.

2.2.1.2 Thermally Responsive Hydrogels

Some hydrogels will shrink when the temperature exceeds a low critical solution temperature (LCST) [24]. One example is PNIPAM (Poly(N-isopropylacrylamide)), which is commonly used as a thermally responsive material for actuation purposes. When the temperature reaches the LCST, a hydrophobic interaction between polymer chains leads to a molecular transition from hydrophilic coil to hydrophobic globule [42], expelling water from the network.

Thermally responsive hydrogels can be actuated by either directly increasing the temperature of the surrounding environment or by incorporating heat generating additives inside the network. Yu and coworkers harnessed the Joule heat generated by embedded electric circuits to control the swelling and deswelling of bulk hydrogel PNIPAM [44]. Hayward's group utilized the surface plasmon resonance of gold nanoparticles to convert light at specific wavelengths into thermal energy to bend [45] or buckle a gel sheet [46]. The responsive wavelength is controlled by the size of the nanoparticles. The near-infrared photothermal property of carbon-based materials such as carbon nanotubes [47] or reduced graphene oxide [48,49] can also be employed to achieve fast, reversible actuation of thermally responsive hydrogels.

S. Armon et al. [23] embedded rigid threads in the top and bottom surfaces of a NIPA gel sheet as fiber reinforcements. When the temperature rises beyond the LCST, the NIPA gel will shrink and twist itself or coil into a helix influenced by the thread restriction (Figure 3a). The transition from pure twisting to spiral helix happens as the shrinking ratio increases, which agrees with the theoretical analysis in which the dimensionless width $\tilde{w}$ is related to the swelling/shrinkage induced curvature κ_0 as $\tilde{w} = w\sqrt{\kappa_0/t}$.

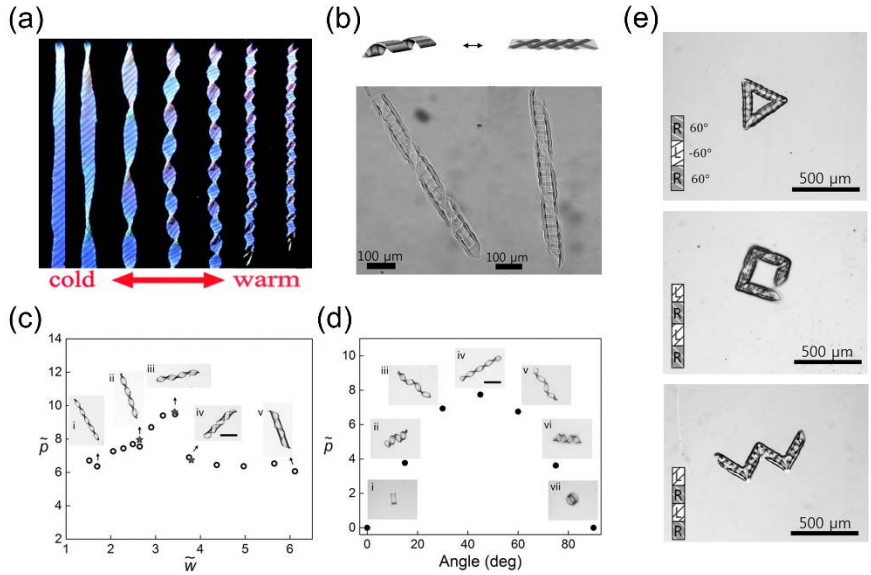

Figure 3. Thermally responsive hydrogel-based helical actuators inspired from *Bauhinia variegate*. (**a**) Transition from a twisted helicoid to a spiral helical shape as the shrinkage ratio of hydrogel increases with rising temperature; (**b**) Schematic illustration of helical transformation in a tri-layer hydrogel composite (top) and a helical hybrid hydrogel with right-handedness (bottom left) or left-handedness (bottom right) under an optical microscope; (**c**) The relationship between the helix pitch and the dimensionless width; (**d**) The relationship between the helix pitch and the reinforcement angle; (**e**) Complex shapes obtained by connecting helices with different lengths or handedness including triangle (top), square (middle) and zigzag (bottom). The insets are 2D precursors of the hydrogel sheets during photo-crosslinking. (**a**) is from Ref. [23], reprinted with permission from The Royal Society of Chemistry; (**b**)-(**e**) are from Ref. [50], reprinted with permission from 2017 Wiley.

Jeon and coworkers [50] photo-crosslink a microscale tri-layer structure where the middle layer is the soft hydrogel poly(N,N-diethylacrylamide-*co*-acrylamidobenzophenone) (PDEAM-BP) sandwiched by two rigid passive polymer layers. The outer layers are parallel strips, and the orientation of strips in one layer is kept orthogonal to those in the other layer. The strip pattern, including the angle relative to the long axis of the ribbon, the width, and the spacing is controlled by a photomask. Upon swelling in a buffer solution, the flat ribbon will coil into a helix (Figure 3b), the handedness, pitch and radius of which are determined by the dimensionless width $\tilde{w}$ and the angle of the parallel strips. This relationship resembles the previous theoretical analysis performed by Armon et al. [9]. A sharp decrease in pitch is found when the dimensionless width exceeds the critical point and thus a twisted shape will transition into a spiral helix (Figure 3c), a 45° tilting angle will produce a twisted helix, and 0° or 90° angle will give a ring shape (Figure 3d). Since the hydrogel is also responsive to heat, increasing temperature will decrease the swelling ratio of the middle layer and untwist the helix.

The patterned strips in Jeon's work play a similar role in determining the final shape to the cellulose fibers in the *Bauhinia variegate* pod. The rigidity of these strips makes the nearby hydrogel swell perpendicular to the strip's direction, and the orthogonal strip alignments in the top and bottom layers form an intrinsic saddle shape which drives the flat ribbon into a helical shape. Optical microscopy images show that the strips on the outer side of the helix orient along the helix axis (Figure 3a) to minimize the stretching and bending in these strips [51].

One advantage of photo-crosslinking is to create an arbitrary 2D geometric pattern with high spatial resolution. More complex shapes at the microscale can be acquired by patterning strips with different angles on specific regions of one monolithic hydrogel ribbon, yielding concatenated helices. Various shapes such as a zigzag, square, or triangle can be produced by tuning the strip angles in different regions (Figure 3e). Jeon et al. also demonstrate that the block angle, torsion angle, and length of the connected helices can be separately programmed, providing a feasible method to fabricate arbitrary 3D curves.

2.2.1.3 pH Responsive Hydrogels

Polymer chains in hydrogels can carry ionic groups, and the network usually stays neutral since the oppositely charged ions balance themselves [24]. However, an environment change such as pH variation will cause the ions to diffuse in or out of the network, resulting in negatively or positively charged chains. The electrostatic repulsion between the charged chains or the destruction of the previous physical crosslinks such as hydrogen bonds increases the interspace, and the hydrogel swells.

Based on the synthesis of an interpenetrating network by photo-crosslinking the monomer solution of one gel in another formed hydrogel matrix, Wang and coworkers [52] use a three-step photopolymerization to fabricate a hybrid hydrogel (Figure 4a). They first photo-crosslink parallel strips of PAA guided by a photomask and leave the strips on the templates. Then they place two templates face to face with an angle between the strip orientations and control the gap using spacers. Injecting a solution of PNIPAM inside the space between the two templates and photo-crosslinking the PNIPAM precursor will form a heterogenous structure which contains an interpenetrating network of PAA/PNIPAM and a single network of PNIPAM. The parallel PAA/PNIPAM strips act

Peer-reviewed version available at Sensors 2018, 18, 2973; doi:10.3390/s18092973

like cellulose fibers while the single network PNIPAM resembles the matrix, mimicking the microstructure of the *Bauhinia variegate* pod. Since PAA/PNIPAM swells in basic solution while PNIPAM is insensitive to base, this composite hydrogel will shift into a helix when pH=9.

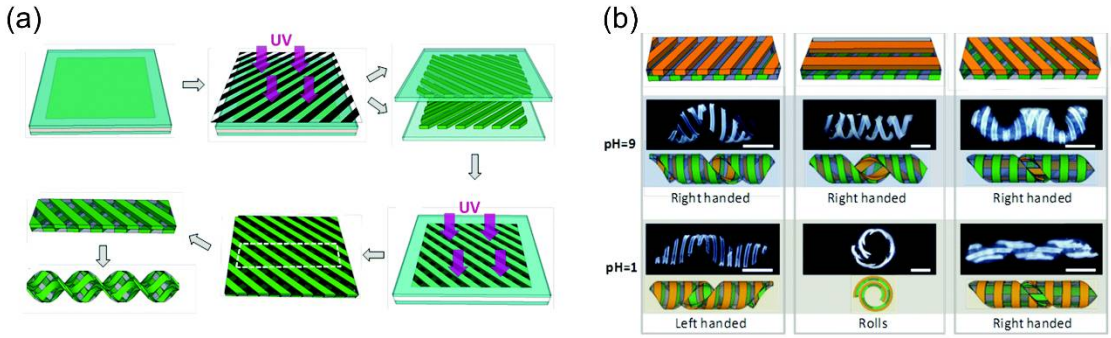

Figure 4. pH-responsive hydrogel-based helical actuators inspired from *Bauhinia variegate*. (**a**) Schematic illustration of the three-step photo-crosslinking of PAA/PNIPAM hybrid composite guided by a photomask. The green strips are PAA while the grey part is PNIPAM. The photomask is made by drawing black lines; (**b**) Shape transformation of P(VI-*co*-AAM)-PNIPAM-PAA hybrid hydrogel when pH changes from 9 to 1. The brown, grey and green parts are P(VI-*co*-AAM), PNIPAM and PAA, respectively. The upper figures show the strip orientations in the top and bottom layers. The helix can change its chirality (left), roll into a circular shape (middle), or flip itself without changing chirality (right) when the strips in top layer swell in an acid environment, shown both in the schematic and experimentally. The scale bar is 1cm. (**a**) and (**b**) are from Ref. [52], reprinted permission from The Royal Society of Chemistry.

The multi-step photopolymerization based on the bonding of new monomers to the existing network makes it easy to integrate multiple stimuli-responsive hydrogels into one monolithic gel, which enables the selective actuation of a single actuator. Wang et al. replace PAA strips in the upper layer with poly(1-vinylimidazole-*co*-acrylamide) (P(VI-*co*-AAM)), which can swell as a response to acids while the bottom layer is kept unchanged. Consequently, changing pH from 9 to 1 can either switch the chirality or flip the helix according to the strip orientation in the top and bottom layers (Figure 4b).

2.2.2. Liquid crystal networks/elastomers-based Actuators

Liquid crystals (LCs) were first recognized as a new phase in 1888 by Austrian botanical physiologist Friedrich Reinitzer, which can flow as liquid while preserve their crystalline molecular structure. This state of matter can not only be found in low-molar-mass chemicals which have revolutionized the display market, but also can be realized in polymeric materials.

Polymers that share the properties of LCs can be categorized into liquid crystal polymers (LCPs), liquid crystal polymer networks (LCNs), and liquid crystal elastomers (LCEs). LCPs have un-crosslinked linear mesogenic groups (which induce the liquid crystal phase to the polymer) and undergo the smallest molecular order change (which leads to deformation at the macroscopic scale) when subjected to stimuli. LCNs have a medium to high crosslink density and have a moderate order change as a response to stimuli. The cross-link density effect on the thermal response of LCN is revealed by Wie et al.: lower density means lower temperature threshold of the thermally-induced shape change and larger deformation [53]. Lastly, LCEs are a subset of LCNs that are lightly crosslinked. Stimuli can trigger relatively large deformations of materials composed of LCE. For detailed information of the microstructure and classification of liquid crystal polymers, please refer to the excellent review paper by White and Broer [54].

LCNs or LCEs can change their shape as a response to external stimuli such as temperature (thermotropic), light (phototropic), or solution concentration (lyotropic), which allows them to function as soft actuators for a wide range of potential applications such as medical devices, microfluidic and microelectromechanical systems, artificial muscles and soft robotics [55–58]. Unlike

the isotropic swelling or shrinkage of hydrogels, LCNs or LCEs can undergo anisotropic responsive deformation which originates from their heterogenous microstructures in which the molecular order is reduced when triggered by external stimuli. This reduction of molecular order will lead to expansion perpendicular to the molecular orientation and contraction along the molecular direction. This anisotropic response is inherent in LCN or LCE microstructures without the introduction of additional reinforcement or the integration of different material compositions, which is a distinct advantage compared to the hydrogel system. Recent progress on designing programmable self-morphing LCNs materials can be found in these extensive reviews [59–65].

For LCNs or LCEs, the shape transition is dictated by the programmable molecular orientation inside the matrix. By orienting the directors along the thickness of the LCN film, various types of LCN can be achieved such as planar-, vertical-, hybrid-, and twist-nematic configurations (Figure 5a). A uniform planar or vertical alignment will lead to a purely planar expansion or contraction while a nonuniform distribution of the director orientation such as the hybrid or twist alignment will buckle the flat sheet into 3D configurations. Urayama summarized studies on thermally triggered deformations including spiral and helix formation that arise from these different types of director configurations [66].

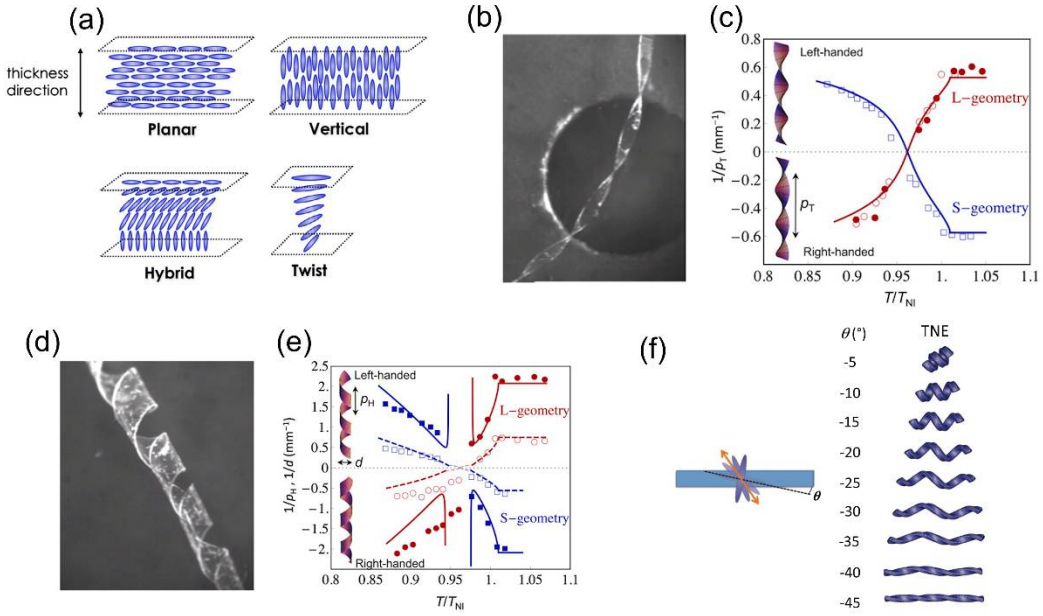

Figure 5. Nematic configurations and formation of helix/spiral induced by temperature variation. **(a)** Planar-, vertical-, hybrid-, and twist-nematic configurations of a LCN; **(b)** Formation of a helicoid ribbon from narrow TNE film at 330 K; **(c)** Inverse of the twist pitch ($1/p_T$) as a function of normalized temperature (T/T_{NI}, where T_{NI} is the nematic-isotropic transition temperature). Positive and negative p_T indicate left- and right handedness, respectively. Red circles and blue squares represent data of L- and S-geometry, respectively. Filled symbols indicate data obtained in cooling processes and open in heating processes. Theoretical predictions are represented by lines; **(d)** Formation of a spiral ribbon from the wide TNE film at 336 K; **(e)** Inverse of the helical pitch ($1/p_h$) and the diameter ($1/d$) as a function of T/T_{NI}. Positive and negative p_H indicate left- and right handedness, respectively. Red circles and blue squares represent data of L- and S-geometry, respectively. Filled symbols are data for $1/d$ and open symbols are data for $1/p_h$. Theoretical predictions are represented by lines; **(f)** Various simulated helical shapes corresponding to different off-axis angles. Simulation performed by Vianney Gimenez-Pinto. (θ). Figure reprinted with permission from: (a) reference [66], Elsevier; (b)-(e) reference [12]; (f) reference [67], American Physical Society.

Among these different microstructures, twist-alignment LCNs or LCEs in which the director rotates left- or right-handedly by an angle (usually 90º) from the bottom to top surface can generate a helical shape in response to stimuli. This actuation behavior resembles seedpod chiral opening and shares a similar mechanism if we only consider the regions near the top and bottom surfaces. The

anisotropic swelling near the top is perpendicular to the bottom due to the orthogonal molecular directions. It creates intrinsic saddle shape which twists the flat sheet into a helix.

In the following sub-sections, we focus on the helical actuations of LCNs or LCEs that mimic the *Bauhinia variegate* pod opening in terms of the responsive stimuli ranging from the most widely used ones, heat and light, to less-frequently used ones including chemical, humidity, and water.

2.2.2.1 Thermally responsive LCNs or LCEs

Heat is the most common stimulus for polymeric LC materials by far in that it can trigger deformation without any additive doped into the material or reliance on a multilayer structure. This inherent property is due to the opposite sign of thermal expansion along different directions of the molecular alignment (director) in the polymer. For example, upon heating, the thermal expansion parallel to the director is negative and much larger than that perpendicular to it in LCE, while in LCN the thermal expansion parallel to the director is negative to and much smaller than that perpendicular to it [54,57,68]. The anisotropic thermomechanical response of LCEs and LCNs are triggered due to the heterogeneity in the direction of local molecular alignment of the material. This is different from other thermally induced mechanical responses that rely on heterogenetic sensitivity to stimuli or compositions, such as a bilayer structure containing a passive layer and an active layer [54].

Sawa et al. studied how the microscopic chiral alignment of mesogens in twisted-nematic-elastomer (TNE) films transfers to the macroscopic formation of helical ribbons [12]. They created TNE films with the director left-handedly rotating by 90° from the bottom to the top surface by photopolymerizing the mesogenic monoacrylate and crosslinker in a nematic solvent with chiral dopants. The mutually perpendicular directors at top and bottom surfaces are formed by corresponding substrates coated by a uniaxially rubbed polyimide layer. They cut out the long ribbon specimen from the film in a way that the director at the middle plane is either parallel to the long axis (L-geometry) or the short axis (S-geometry) of the ribbon.

Through both experimental observation and theoretical modeling, they find that for both the S- and L-geometry, the width of the specimen determines what shape it forms. A narrow ribbon forms a helicoid (Figure 5b) and a wide one forms a spiral ribbon (Figure 5d). This behavior resembles that of a seedpod and can be explained by the domination of the bending energy (in the narrow case) or the stretching energy (in the wide case) as discussed in section 2.1. Quantitative models capturing the transition from helical to spiral structure in a TNE ribbon have also been proposed [69,70]. In the narrow case, temperature variation will change the twist pitch (p_T) of the helicoid (Figure 5c). In the wide case, it will change the helical pitch (p_H) and diameter (d) of the spiral ribbon (Figure 5e). In both cases (Figure 5c, 5e), handedness reversions are involved and the shape changing processes are thermally reversible. The structural parameters (e.g. p_T, p_H, and d) of the TNE ribbons are no longer dependent on temperature variation once it is greater than the nematic-isotropic transition temperature (T_{NI} = 367K).

Intuitively, one might ask what shapes TNE ribbons will form if the director at the mid-plane of the film is not along the long or the short axis of the ribbon (i.e. not S- or L-geometry). Sawa et al. examine the shape evolution of off-axis TNE ribbons as a function of temperature using experiments and finite element analysis (FEA) [67]. They show that when the director at the mid-plane is off axis, the ribbon will not shape into helicoids but into distorted spiral ribbons. They predict the varying spiral shapes with respect to different off-axis angles (θ) using FEA simulation (Figure 5f).

The formed helix/spiral shape of the TNE upon heating will return to its original shape immediately upon removal of the heat source. Lee et al. designed an autonomous shape fixing procedure that retains the spiral ribbon structure of a TNE film even after the heat stimulus is removed [71]. This hands-free shape fixing ability is obtained by rapid cooling. In a dynamic mechanical analysis, they demonstrate that this technique retains up to 96% of the strain (an indicator of deformation) in the shape after cooling. Furthermore, if the formed shape is under an external mechanical constraint (e.g. tweezers and adhesions) the cooling rate can be moderately slower.

Researchers have investigated many other mechanisms based on the planar patterning leading to helical/spiral actuation using a single-layer LCE film. By using photopatterning techniques, spatial

variation of the domain orientation in monolithic TNE films [71] and dual-phase (nematic and isotropic) monolithic LCE films [72] have been fabricated to form helical shapes. The shape transformation can also be achieved by assigning LCE films with different compositions or nematic configurations [73]. Finally, instead of using single-layer twist nematic LCNs, LCEs are used in bi-layer structures to form helical/spiral ribbons. Agrawal et al. have constructed a LCE-polystyrene bilayer, in which the polystyrene (serving as the constraining layer) is deposited on the LCE film with a certain angle and curls into a helical shape upon heating [74]. Boothby and colleagues have also designed a bilayer structure that is composed of a layer of hydrophilic polymer (serving as the constraining layer) and a layer of LCE [75]. As temperature increases, the LCE layer stretches in the direction perpendicular to the molecular director which is 45º to the long axis of the LCE ribbon, leading to a helicoid. When the temperature drops to room temperature, a spiral ribbon is formed.

2.2.2.2 Light-responsive LCNs or LCEs

Light is another attractive source of stimulus to induce a macroscale mechanical response of LCNs because it is readily available, versatile, and controllable. An increasing number of studies have investigated the conversion of light into motion of LC-based soft actuators [54,55,76]. We only focus on those works that produce motions mimicking the opening of seedpod (i.e. the formation of a 3D helical/spiral structure from a 2D ribbon).

A detailed preparation protocol for an LCN based photo-responsive soft actuator is described by Iamsaard et al. [77]. Briefly, azobenzene is introduced into the LCN's covalent structure to serve as a molecular photochromic switch. The host matrix is a mix of low molecular-weight nematic LC, acrylate-functionalized nematic LC, and a photoinitiator. The mixture is doped with chiral dopants that generate a 90° smooth twist between the top and bottom surfaces.

The formation of a helical shape of this material induced by ultraviolet (UV) light was observed in 2005 [78]. Later, researchers deliberately studied the winding and unwinding motion of the helix formed by LCN ribbons [79]. As shown in Figure 6a, in addition to the findings on how the ribbon cutting angle (φ) determines the pitch and handedness of the helical shape, Iamsaard and colleagues have some interesting new discoveries. They observe that under irradiation with UV light the helical pitch decreases in left-handed ribbons and increases in right-handed ribbons and therefore large contractions and elongations of the ribbon are generated. They also witness the inversion of the helix from right-handed to left-handed when the ribbon is irritated by UV light at large cutting angle. Similar to the mechanism of deformation induced by heat, these shape changes of LCN with photoresponsive dopants irradiated by light are consequences of anisotropic deformation at a microscopic level: molecules contract along the director and expand in perpendicular direction (Figure 6b).

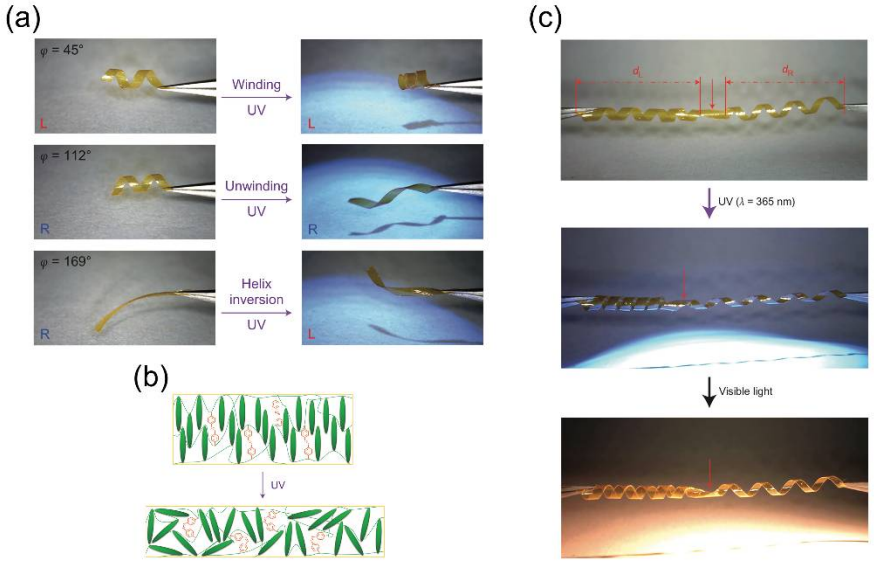

Figure 6. Light-induced helical motion. **(a)** Change in pitch and inversion of handedness of spiral ribbons cut at different angles (φ) irradiated by UV light; **(b)** Anisotropic deformation at the molecular level: shrinkage along the director and expansion in the direction perpendicular to the director; **(c)** A proof-of-principle for an actuator capable of performing complex motion: the kink in the middle connecting helices of opposite handedness shows a smooth push-pull motion. Figure reprinted by permission from reference [79], Springer Nature.

The authors demonstrate a proof-of-concept of a photomechanical actuator in response to alternating UV and visible light. This actuator consists of an LCN-based ribbon with opposite handedness on two sides connected by a kink that performs continuous push-pull motions like a piston (Figure 6c). Finally, a biomimetic bilayer soft actuator is developed using LCE that can perform chiral twisting motions when irradiated by UV [80]. The top and bottom ribbon layers have different photo-responsive properties and are glued to each other with a tilted angle (Fig. 5e). This angle determines the chirality of the formed helix (Fig. 5f).

2.2.2.3 Other stimuli-responsive LCNs or LCEs

Other stimuli that actuate LC based shape transformations also have caught researcher's attention in recent years. We briefly review several examples of actuations by chemical-, humidity-, water-, and magnetic- stimuli.

Boothby et al. have examined LCEs as chemoresponsive actuators [81]. They experimentally show that TNE ribbons form into twisted shapes in response to tetrahydrofuran (THF) as the chemical stimulus in liquid or in vapor form (Figure 7a). This TNE can even carry a weight 100 times heavier than itself and twist into a helicoid and a helix as a function of time (Figure 7b).

Peer-reviewed version available at Sensors 2018, 18, 2973; doi:10.3390/s18092973

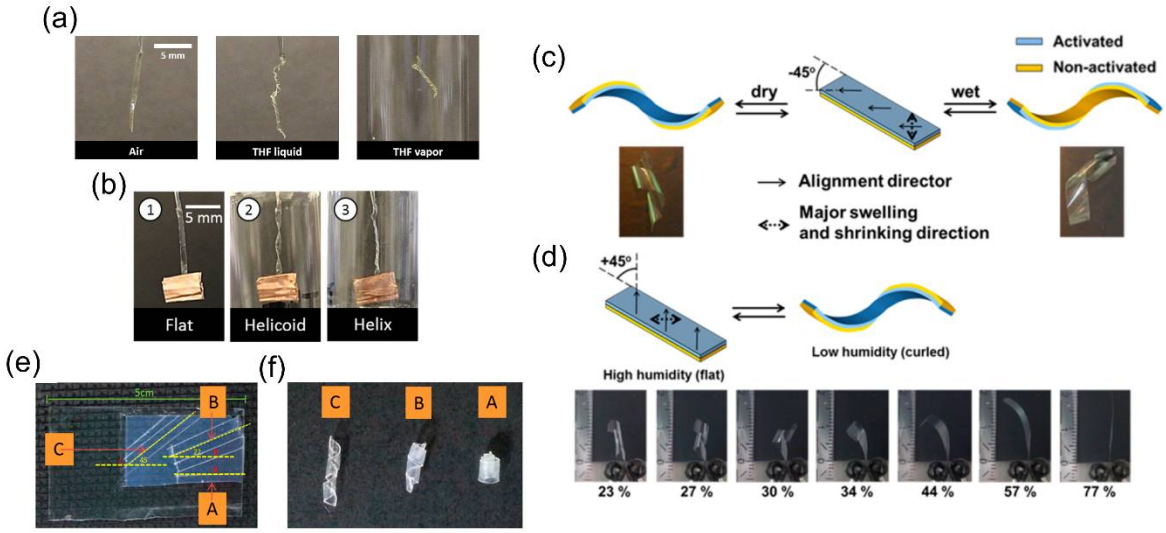

Figure 7. Formation of a helical shape triggered by other stimuli. **(a)** TNE ribbon in air, THF liquid, and THF vapor; **(b)** TNE ribbon remaining flat in air and curling into a helicoid and a self-contacting helix in THF vapor as a function of time; **(c)** A bilayer LCN ribbon, in which the director is 45º to the long axis of the ribbon, showing left-handedness when dried and right-handedness when wet; **(d)** A bilayer LCN ribbon, in which the director is -45º to the long axis of the ribbon, exhibiting a smooth transition in shape from flat to curled as humidity decreases; **(e)** Ribbons cut at different angles (A: 0 º; B: 22 º; C: 45 º) on a single-layer LCE film in which the director is in the horizontal direction; **(f)** Formation of different helically coiled shapes of A, B and C in response to water exposure. Figure reprinted with permission from: (a) and (b) reference [81], Elsevier; (c) and (d) reference [82], American Chemical Society; (e) and (f) reference [83], American Chemical Society.

Humidity in air has proven to be an effective controlling parameter to determine the extent of curling of an LC polymer. Instead of using a monolithic TNE ribbon, a bilayer planar aligned LCN ribbon is fabricated by De Haan et al. [82]. The two layers are attached to each other in a way that the angle between their directors and the long axis of the ribbon is -45° (Figure 7c). When the ribbon is wet on the activated side, it curls into a right-handed helix, and when it is dried, it reverses to a left-handed helix. When the angle is 45°, however, the ribbon is flat when it is exposed to high humidity and right-handed when exposed to low humidity. This asymmetry is achieved by locally converting the uniaxially aligned LCN film to a hygroscopic polymer salt that swells perpendicular to the director. It is also shown that the extent of curling of the specimen depends on the humidity level it is exposed to (Figure 7d).

A single-layer actuator based on LCE that changes shapes in response to water/acetone is designed by Kamal and Park [83]. The asymmetric deformation (including forming a spiral shape) of the LCE-based ribbon mainly arises from the nematic-isotropic transition and a porous gradient in the thickness direction (i.e. during photopolymerization, the UV-exposed side is smooth while the other side is highly porous). After a straight ribbon is cut from the LCE film and immersed in water, it will form a spiral shape of a certain pitch depending on the angle between the long axis of the ribbon and the orientation of the director of the LCE (Figure 7e, 7f). This process is reversed when the curled ribbon is immersed in acetone.

Lastly, via incorporating magnetic nanoparticles in LCE-based materials, soft actuators stimulated by magnetics field can be obtained [84–86]. However, this technique has not yet been used to enable helical/spiral shape formation.

2.2.3. Shape Memory Polymers-based Actuators

Shape memory polymers (SMPs) which can switch from a temporary state to a permanent state under external stimuli such as heat [87] or specific chemical solution [88] are widely used in actuation

systems since the shape transformation is usually predictable and easily programmed [89,90]. Although shape memory polymers have a wide variety of possible shape-change mechanisms, they generally involve a glass transition temperature T_g. Below this temperature, the polymer is stiff and glassy, while above it the polymer is rubbery and can flow to relax the internal residue stress. Typically, to employ the memory effect of SMPs to achieve actuation, one needs to deform the initially stress-free shape memory polymers and then decrease the temperature below T_g, during which the deformation needs to be held at all time. After this shape fixing stage, due to the interaction between polymer chains, SMPs cannot recover to the previous shape. When the temperature is later increased above T_g, the polymer chains can then slip with each other like rubble and SMPs can thus relax the internal stress and deform back to its permanent configuration [91].

Based on the shaping fixing and recovery of SMPs, Robertson and coworkers [92] fabricate a shape memory laminated composite which can coil into a helix upon heating. During the fabrication process, they first electrospin aligned poly(vinyl acetate) (PVAc) fibers guided by the electric filed and then infiltrate the fiber's interspace with poly(dimethylsiloxane) (PDMS) precursor (Figure 8a). A single-layer elastomeric composite reinforced with unidirectional fibers is obtained after curing process, which is later used to fabricate a bilayer mat by adhering two single-layer laminas. The adhesion is realized via curing the uncrosslinked PDMS and the tilting angle between the fiber's directions in two layers can be tuned before the stacking step.

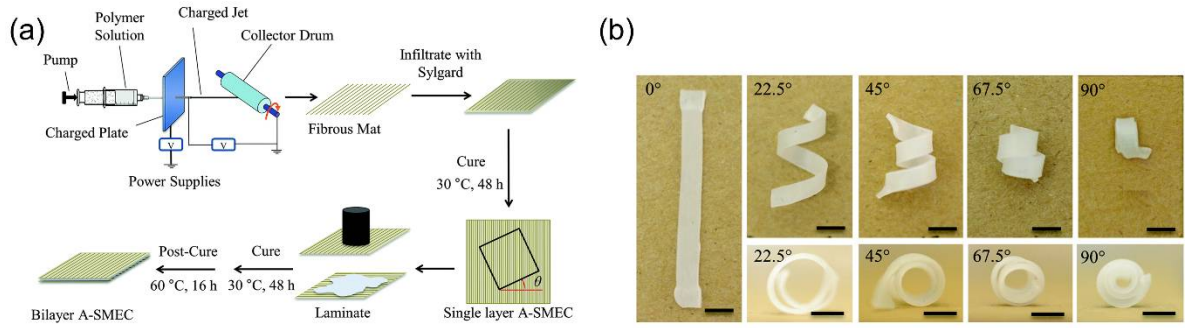

Figure 8. Shape memory polymers-based helical actuator inspired from *Bauhinia variegate*. **(a)** Schematic illustration of the fabrication process of the shape memory elastomeric composite; **(b)** Experimental images of the coiled bilayer composites after heat treatment. The radius and pitch depend on the tilting angel between fiber's directions in two layers. The left corner of each image shows the tilting angel and the scale bar is 4mm. (a) and (b) are from Ref. [92], reprinted with permission from The Royal Society of Chemistry.

The shape memory effect of this composite relies on the shape recovery of the PDMS matrix and shape fixing ability of PVAc fibers. PVAc fibers can develop plastic strain below T_g and relax it when the temperature exceeds the critical point. Therefore, the mechanical stretching below T_g of the laminate composite will produce plastic strain inside PVAc fibers which then get relaxed during the heating treatment. Because of the tilting angle between fiber reinforcements in two layers, the strain relaxation leads to mechanical frustration and coils the composite sheet into a spiral shape like the pod's opening of *Bauhinia variegate*. They also find that the variation of the tilting angle will change the pitch and radius of the spiral shape, sharing the similar behavior with other seedpod-inspired synthetic actuators (Figure 8b).

3. Helical Actuators Inspired from *Towel Gourd* Tendril's Coiling

3.1. Coiling Mechanism of Towel Gourd Tendrils

In addition to the chiral pod opening of *Bauhinia variegate*, another vivid example in the plant kingdom which exhibits helical shape evolution is tendril coiling, whereby an initially straight tendril can not only coil into a spiral shape but also develop co-existing left-handed and right-handed segments connected by perversions for enhanced structural support [10]. Once it attaches to a

Peer-reviewed version available at Sensors 2018, 18, 2973; doi:10.3390/s18092973

support, an asymmetrical contraction of fibers will form an intrinsic curvature by virtue of differential lignification, water transportation, and orientation of cellulose fibrils. It will further wind the tendril to pull itself to a higher place for more sunshine, since twisting is energetically favorable versus bending, and the perversion is always formed due to a topological constraint (Figure 9a) [93]. For further information with respect to perversion formation, readers can refer to Ref. [94–99].

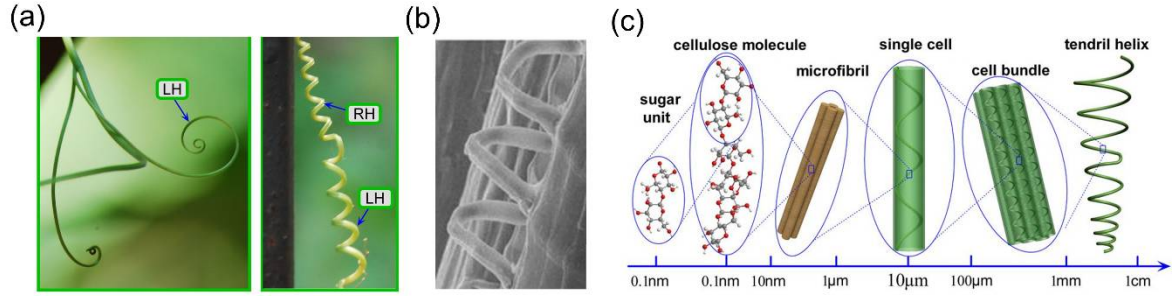

Figure 9. Coiling mechanism of *Towel Gourd* tendrils. **(a)** *Towel Gourd* tendril coils into a spiral shape with left-handedness when the end is free (left) and forms a perversion connecting the right-handed and left-handed sections once it attaches to a support. 'LH' and 'RH' represent left-handed and right-handed, respectively; **(b)** Image of helical cellulose fibril inside cell's matrix under scanning electron microscope; (**c**) Hierarchical chirality inside *Towel Gourd* tendril from the molecular level to the macroscopic shape. (**a**)-(**c**) are from Ref. [10], reprinted permission from Nature Publishing Group.

Tendril perversion provides inspirations for a number of engineered structures with interesting mechanical properties. For example, Gerbode et al. [93] designed twistless springs by bonding two layers of differentially pre-stretched silicone rubber sheets cut along the uni-axial pre-stretch direction. The ribbon hence has an intrinsic curvature and will form a twistless spring with a left-handed and a right-handed helix segment connected by a perversion when it is clamped at both ends and stretched axially. They also systematically investigated the unwinding and overwinding behavior of the physical model and the tendril fiber ribbons, and concluded that the existence of intrinsic curvature, topological constraints, mechanical asymmetry and the large bending rigidity to twist rigidity ratio together contributed to the interesting springy behavior of the tendril structure. Liu et al. [94] and Huang et al. [97] used a similar physical model but further established theoretical and finite element analysis on the formation of hemihelices. They found that for bilayer strips with a rectangular cross-section the formation and the number of hemihelices depend on the aspect ratio of the cross-section, thus providing the basis for designing springs made of these hemileces from initially flat strips. Chen [99] further explored the possibility of generating perversions in bilayer strips in strained nanostructures with and without clamped boundary conditions.

Tendrils can also coil without attaching to a support, which can be attributed to the internal chiral building blocks. This chiral transfer mechanism in which the chiral molecules or microstructures contribute to a helical macroscopic morphologies has also been observed in other species, such as the hydroscopic coiling of the stork's bill awns [100]. For the coiling of *Towel Gourd* tendrils, Wang and coworkers discover a hierarchical chirality transfer mechanism across different length scales from the molecular level to the macroscopic (Figure 9c). During swelling or deswelling, the helical angle of the reinforced cellulose fibrils inside the rod-like cell's matrix (Figure 9b) will change and introduce an internal torque on the tendril's cross-section [101], which is believed to drive the tendril's coiling during its biological growth.

In the following sub-section, we provide a small-scale review on carbon nanotube (CNT)-based helical actuators inspired from the coiling of *Towel Gourd* tendrils. Unlike the aforementioned planar-to-helical transformation, this class of helical actuators focuses on the winding and unwinding of a helical structure to create a contraction or rotary actuation mode.

3.2. Actuators Inspired from Towel Gourd Tendrils

Peer-reviewed version available at Sensors 2018, 18, 2973; doi:10.3390/s18092973

Carbon nanotubes (CNT) are well-known for their outstanding mechanical and electrical properties, and it has been demonstrated that twist-spun multiwalled carbon nanotubes (MWCNTs) with filled hosts can provide rapid contraction and rotary motion under different stimuli which exceed the performance of conventional artificial muscles [102,103].

Inspired by the hierarchical structure in *Towel Gourd* tendrils, Peng's group [13,104] fabricate hierarchical helical fibers (HHFs) by two-level twisting of MWCNTs. They first synthesize the primary fibers with helical alignment of MWCNTs using dry-spinning, then twist the multi-ply primary fibers. Once the twisting reached a critical value, the bundled primary fibers will coil compactly into a stable fiber without partial untwisting (Figure 10a).

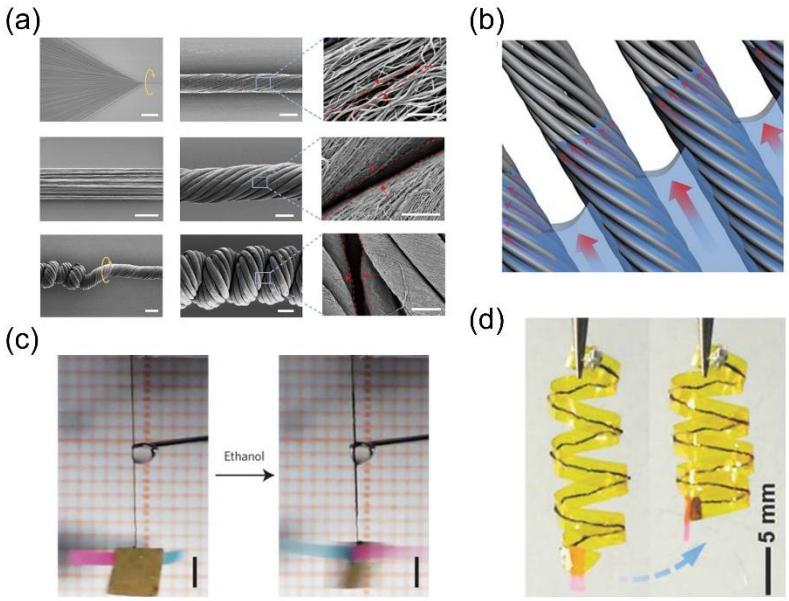

Figure 10. CNT-based helical actuators inspired from *Towel Gourd* tendrils. **(a)** Groups of scanning electron images showing the fabrication process of the hierarchical helical fibers based on twisting MWCNTs. First step is to dry-spin MWCNTs into a helical alignment to form a primary fiber (first row: dry-spinning (left, scale bar 500μm), primary fiber (middle, scale bar 10μm) and the nanoscale gaps between MWCNTs (right, scale bar 500nm)). The next step is to twist the multi-ply primary fibers (second row: bundle of primary fibers (left, scale bar 200μm), twisted primary fibers (middle, scale bar 30μm) and the microscale gaps between primary gaps (right, scale bar 2μm)) until it reaches a critical point beyond which the bundle will coil into a helical shape (third row: coiling when twisting exceeds the threshold (left, scale bar 50μm), hierarchical helical fiber (middle, scale bar 30μm) and gaps inside HHF (right, scale bar 10μm)); **(b)** Hierarchical gaps, including microscale gaps between primary fibers and nanoscale gaps between MWCNTs, facilitate the solution's infiltration; (**c**) The contraction actuation of the hierarchical helical fiber when contacting an ethanol drop. It can contract and rotate the copper paddle. The left image is the HHFs before contacting ethanol while the right image is the snapshot after 1.63s when it touches ethanol. Scale bar is 2mm; (**d**) Electromechanical contraction actuation of a left-handed Kapton film with HHF inside. (**a**) is from Ref. [104], reprinted permission from Nature Publishing Group; (**b**)-(**c**) are from Ref. [13], reprinted permission from Nature Publishing Group; (**d**) is from Ref. [105], reprinted permission from 2015 Wiley.

The fabricated HHFs can contract or rotate when contacting the polar solvent or when exposed to its vapor (Figure 10c). The actuation mechanism comes from the gaps inside the structure. They provide space for solution infiltration, which expands the structure and initiates motion as a result.

It was discovered that the hierarchical helical structure in HHFs contains gaps across two length scales, which are the nanoscale gaps between the MWCNTs and the microscale gaps between the primary fibers. The combination of these two-level gaps facilitates the fast infiltration of the polar solution (Figure 10b) and stabilizes the fiber integrity during periodic twisting and untwisting.

Owing to this, the HHFs can achieve rapid, reversible contraction and rotation with a prolonged working life, which is not achievable when only nanoscale gaps exist.

Relying on the hierarchical structure in HHFs, Peng's group [105] also harness the electromagnetic interaction between aligned CNTs to realize electromechanical actuation of HHFs, whose performance is better than the previously reported electrothermal or electrochemical actuation in terms of the power output, actuation speed, and stability. Apart from the 1D contraction, they use a heat-setting process to fix the HHFs into a helix and sew them into a Kapton film. The helical integrated structure will wind or unwind itself when it receives an electrical signal, which mimics the tendril's coiling process (Figure 10c).

4. Summary and Outlook

Bioinspired helical actuators have shown fascinating performance such as the construction of a programmable helical shape or tunable winding/unwinding behavior by controlling the external stimuli, which greatly broadens the feasible pathways to the future applications. The opening mechanism of the *Bauhinia variegate* pod offers a universal principle for the generation of helical shape, that is, to create an intrinsic doubly-curved shape with a misorientation angle between the principal axes and the geometric axes. The microstructure of the *Bauhinia variegate* pod also enlightens us to utilize composition heterogeneity (i.e. aligned rigid reinforcements or molecular orientations) to generate anisotropic responses, which play a crucial role in the formation of tunable three-dimensional structures. Such strategy relaxes the reliance on anisotropic material properties, which significantly expands the design space stimuli-responsive materials. For instance, the hierarchical chirality transfer mechanism in the coiling of *Towel Gourd* tendrils promotes the development of CNTs-based actuators by forming gaps across two different length scales.

Although significant advances have been made in the synthesized actuators inspired by these plant structures, some unique properties originating from the shape-shifting mechanisms have still not been fully exploited for better functionality, such as bistability [9, 21, 22, 106]. For example, for the helical shape transformation driven by the intrinsic saddle shape, two stable solutions emerge when the ribbon is wide enough or thin enough, and two stable helices can exist under the same condition. The switch between these two stable states, the so-called snap-through, is of great benefit in terms of achieving fast and large actuation without continuing energy input. To the authors' knowledge it has not been extensively used to realize fast snaps of helical actuators. The integration of such stimuli-responsive structure with smart materials will likely provide a much enriched design space for smart structures and devices with a broad range of applications.

Acknowledgments: Z.C. acknowledges the startup fund from the Thayer School of Engineering and the Branco Weiss—Society in Science fellowship (administered by ETH Zürich).

Conflicts of Interest: The authors declare no conflict of interest.

References

1. Mosadegh, B.; Polygerinos, P.; Keplinger, C.; Wennstedt, S.; Shepherd, R. F.; Gupta, U.; Shim, J.; Bertoldi, K.; Walsh, C. J.; Whitesides, G. M. Pneumatic Networks for Soft Robotics that Actuate Rapidly. *Advanced Functional Materials* **2014**, *24*, 2163–2170, doi:10.1002/adfm.201303288.
2. Overvelde, J. T. B.; de Jong, T. A.; Shevchenko, Y.; Becerra, S. A.; Whitesides, G. M.; Weaver, J. C.; Hoberman, C.; Bertoldi, K. A three-dimensional actuated origami-inspired transformable metamaterial with multiple degrees of freedom. *Nature Communications* **2016**, *7*, 10929, doi:10.1038/ncomms10929.
3. Felton, S.; Tolley, M.; Demaine, E.; Rus, D.; Wood, R. A method for building self-folding machines. *Science* **2014**, *345*, 644–646, doi:10.1126/science.1252610.

4. Jung, W.; Choi, S. M.; Kim, W.; Kim, H.-Y. Reduction of granular drag inspired by self-burrowing rotary seeds. *Physics of Fluids* **2017**, *29*, 041702, doi:10.1063/1.4979998.
5. Chattopadhyay, S.; Moldovan, R.; Yeung, C.; Wu, X. L. Swimming efficiency of bacterium Escherichia coli. *Proceedings of the National Academy of Sciences* **2006**, *103*, 13712–13717, doi:10.1073/pnas.0602043103.
6. Tottori, S.; Zhang, L.; Qiu, F.; Krawczyk, K. K.; Franco-Obregón, A.; Nelson, B. J. Magnetic Helical Micromachines: Fabrication, Controlled Swimming, and Cargo Transport. *Advanced Materials* **2012**, *24*, 811–816, doi:10.1002/adma.201103818.
7. Xu, S.; Yan, Z.; Jang, K.-I.; Huang, W.; Fu, H.; Kim, J.; Wei, Z.; Flavin, M.; McCracken, J.; Wang, R.; Badea, A.; Liu, Y.; Xiao, D.; Zhou, G.; Lee, J.; Chung, H. U.; Cheng, H.; Ren, W.; Banks, A.; Li, X.; Paik, U.; Nuzzo, R. G.; Huang, Y.; Zhang, Y.; Rogers, J. A. Assembly of micro/nanomaterials into complex, three-dimensional architectures by compressive buckling. *Science* **2015**, *347*, 154–159, doi:10.1126/science.1260960.
8. Timoshenko, S. Analysis of Bi-Metal Thermostats. *Journal of the Optical Society of America* **1925**, *11*, 233, doi:10.1364/JOSA.11.000233.
9. Armon, S.; Efrati, E.; Kupferman, R.; Sharon, E. Geometry and Mechanics in the Opening of Chiral Seed Pods. *Science* **2011**, *333*, 1726–1730, doi:10.1126/science.1203874.
10. Wang, J.-S.; Wang, G.; Feng, X.-Q.; Kitamura, T.; Kang, Y.-L.; Yu, S.-W.; Qin, Q.-H. Hierarchical chirality transfer in the growth of Towel Gourd tendrils. *Scientific Reports* **2013**, *3*, doi:10.1038/srep03102.
11. Sydney Gladman, A.; Matsumoto, E. A.; Nuzzo, R. G.; Mahadevan, L.; Lewis, J. A. Biomimetic 4D printing. *Nature Materials* **2016**, *15*, 413–418, doi:10.1038/nmat4544.
12. Sawa, Y.; Ye, F.; Urayama, K.; Takigawa, T.; Gimenez-Pinto, V.; Selinger, R. L. B.; Selinger, J. V. Shape selection of twist-nematic-elastomer ribbons. *Proceedings of the National Academy of Sciences* **2011**, *108*, 6364–6368, doi:10.1073/pnas.1017658108.
13. Chen, P.; Xu, Y.; He, S.; Sun, X.; Pan, S.; Deng, J.; Chen, D.; Peng, H. Hierarchically arranged helical fibre actuators driven by solvents and vapours. *Nature Nanotechnology* **2015**, *10*, 1077–1083, doi:10.1038/nnano.2015.198.
14. Forterre, Y.; Skotheim, J. M.; Dumais, J.; Mahadevan, L. How the Venus flytrap snaps. *Nature* **2005**, *433*, 421–425, doi:10.1038/nature03185.
15. Reyssat, E.; Mahadevan, L. Hygromorphs: from pine cones to biomimetic bilayers. *Journal of The Royal Society Interface* **2009**, *6*, 951–957, doi:10.1098/rsif.2009.0184.
16. Elbaum, R.; Zaltzman, L.; Burgert, I.; Fratzl, P. The Role of Wheat Awns in the Seed Dispersal Unit. *Science* **2007**, *316*, 884–886, doi:10.1126/science.1140097.
17. Li, S.; Wang, K. W. Plant-inspired adaptive structures and materials for morphing and actuation: a review. *Bioinspiration & Biomimetics* **2016**, *12*, 011001, doi:10.1088/1748-3190/12/1/011001.
18. Forterre, Y.; Dumais, J. Generating Helices in Nature. *Science* **2011**, *333*, 1715–1716, doi:10.1126/science.1210734.

19. Pezzulla, M.; Smith, G. P.; Nardinocchi, P.; Holmes, D. P. Geometry and mechanics of thin growing bilayers. *Soft Matter* **2016**, *12*, 4435–4442, doi:10.1039/C6SM00246C.
20. Alben, S.; Balakrisnan, B.; Smela, E. Edge Effects Determine the Direction of Bilayer Bending. *Nano Letters* **2011**, *11*, 2280–2285, doi:10.1021/nl200473p.
21. Guo, Q.; Mehta, A. K.; Grover, M. A.; Chen, W.; Lynn, D. G.; Chen, Z. Shape selection and multi-stability in helical ribbons. *Applied Physics Letters* **2014**, *104*, 211901, doi:10.1063/1.4878941.
22. Chen, Z.; Guo, Q.; Majidi, C.; Chen, W.; Srolovitz, D. J.; Haataja, M. P. Nonlinear Geometric Effects in Mechanical Bistable Morphing Structures. *Physical Review Letters* **2012**, *109*, doi:10.1103/PhysRevLett.109.114302.
23. Armon, S.; Aharoni, H.; Moshe, M.; Sharon, E. Shape selection in chiral ribbons: from seed pods to supramolecular assemblies. *Soft Matter* **2014**, *10*, 2733, doi:10.1039/c3sm52313f.
24. Ahn, S.; Kasi, R. M.; Kim, S.-C.; Sharma, N.; Zhou, Y. Stimuli-responsive polymer gels. *Soft Matter* **2008**, *4*, 1151, doi:10.1039/b714376a.
25. Jeon, S.-J.; Hauser, A. W.; Hayward, R. C. Shape-Morphing Materials from Stimuli-Responsive Hydrogel Hybrids. *Accounts of Chemical Research* **2017**, *50*, 161–169, doi:10.1021/acs.accounts.6b00570.
26. Ionov, L. Biomimetic Hydrogel-Based Actuating Systems. *Advanced Functional Materials* **2013**, *23*, 4555–4570, doi:10.1002/adfm.201203692.
27. Kim, J.; Hanna, J. A.; Hayward, R. C.; Santangelo, C. D. Thermally responsive rolling of thin gel strips with discrete variations in swelling. *Soft Matter* **2012**, *8*, 2375, doi:10.1039/c2sm06681e.
28. Kim, J.; Hanna, J. A.; Byun, M.; Santangelo, C. D.; Hayward, R. C. Designing Responsive Buckled Surfaces by Halftone Gel Lithography. *Science* **2012**, *335*, 1201–1205, doi:10.1126/science.1215309.
29. Byun, M.; Santangelo, C. D.; Hayward, R. C. Swelling-driven rolling and anisotropic expansion of striped gel sheets. *Soft Matter* **2013**, *9*, 8264, doi:10.1039/c3sm50627d.
30. Hu, Z.; Zhang, X.; Li, Y. Synthesis and Application of Modulated Polymer Gels. *Science* **1995**, *269*, 525–527, doi:10.1126/science.269.5223.525.
31. Na, J.-H.; Evans, A. A.; Bae, J.; Chiappelli, M. C.; Santangelo, C. D.; Lang, R. J.; Hull, T. C.; Hayward, R. C. Programming Reversibly Self-Folding Origami with Micropatterned Photo-Crosslinkable Polymer Trilayers. *Advanced Materials* **2015**, *27*, 79–85, doi:10.1002/adma.201403510.
32. Wu, Z. L.; Moshe, M.; Greener, J.; Therien-Aubin, H.; Nie, Z.; Sharon, E.; Kumacheva, E. Three-dimensional shape transformations of hydrogel sheets induced by small-scale modulation of internal stresses. *Nature Communications* **2013**, *4*, doi:10.1038/ncomms2549.
33. Thérien-Aubin, H.; Wu, Z. L.; Nie, Z.; Kumacheva, E. Multiple Shape Transformations of Composite Hydrogel Sheets. *Journal of the American Chemical Society* **2013**, *135*, 4834–4839, doi:10.1021/ja400518c.

34. Thérien-Aubin, H.; Moshe, M.; Sharon, E.; Kumacheva, E. Shape transformations of soft matter governed by bi-axial stresses. *Soft Matter* **2015**, *11*, 4600–4605, doi:10.1039/C5SM00561B.
35. Yu, X.; Zhang, L.; Hu, N.; Grover, H.; Huang, S.; Wang, D.; Chen, Z. Shape formation of helical ribbons induced by material anisotropy. *Applied Physics Letters* **2017**, *110*, 091901, doi:10.1063/1.4977090.
36. Studart, A. R.; Erb, R. M. Bioinspired materials that self-shape through programmed microstructures. *Soft Matter* **2014**, *10*, 1284–1294, doi:10.1039/C3SM51883C.
37. Zhang, L.; Chizhik, S.; Wen, Y.; Naumov, P. Directed Motility of Hygroresponsive Biomimetic Actuators. *Advanced Functional Materials* **2016**, *26*, 1040–1053, doi:10.1002/adfm.201503922.
38. Bargardi, F. L.; Le Ferrand, H.; Libanori, R.; Studart, A. R. Bio-inspired self-shaping ceramics. *Nature Communications* **2016**, *7*, 13912, doi:10.1038/ncomms13912.
39. Erb, R. M.; Sander, J. S.; Grisch, R.; Studart, A. R. Self-shaping composites with programmable bioinspired microstructures. *Nature Communications* **2013**, *4*, doi:10.1038/ncomms2666.
40. Ge, Q.; Qi, H. J.; Dunn, M. L. Active materials by four-dimension printing. *Applied Physics Letters* **2013**, *103*, 131901, doi:10.1063/1.4819837.
41. Erb, R. M.; Libanori, R.; Rothfuchs, N.; Studart, A. R. Composites Reinforced in Three Dimensions by Using Low Magnetic Fields. *Science* **2012**, *335*, 199–204, doi:10.1126/science.1210822.
42. Liu, Y.; Takafuji, M.; Ihara, H.; Zhu, M.; Yang, M.; Gu, K.; Guo, W. Programmable responsive shaping behavior induced by visible multi-dimensional gradients of magnetic nanoparticles. *Soft Matter* **2012**, *8*, 3295, doi:10.1039/c2sm07206h.
43. Morales, D.; Bharti, B.; Dickey, M. D.; Velev, O. D. Bending of Responsive Hydrogel Sheets Guided by Field-Assembled Microparticle Endoskeleton Structures. *Small* **2016**, *12*, 2283–2290, doi:10.1002/smll.201600037.
44. Yu, C.; Duan, Z.; Yuan, P.; Li, Y.; Su, Y.; Zhang, X.; Pan, Y.; Dai, L. L.; Nuzzo, R. G.; Huang, Y.; Jiang, H.; Rogers, J. A. Electronically Programmable, Reversible Shape Change in Two- and Three-Dimensional Hydrogel Structures. *Advanced Materials* **2013**, *25*, 1541–1546, doi:10.1002/adma.201204180.
45. Zhou, Y.; Hauser, A. W.; Bende, N. P.; Kuzyk, M. G.; Hayward, R. C. Waveguiding Microactuators Based on a Photothermally Responsive Nanocomposite Hydrogel. *Advanced Functional Materials* **2016**, *26*, 5447–5452, doi:10.1002/adfm.201601569.
46. Hauser, A. W.; Evans, A. A.; Na, J.-H.; Hayward, R. C. Photothermally Reprogrammable Buckling of Nanocomposite Gel Sheets. *Angewandte Chemie International Edition* **2015**, *54*, 5434–5437, doi:10.1002/anie.201412160.
47. Zhang, X.; Pint, C. L.; Lee, M. H.; Schubert, B. E.; Jamshidi, A.; Takei, K.; Ko, H.; Gillies, A.; Bardhan, R.; Urban, J. J.; Wu, M.; Fearing, R.; Javey, A. Optically- and Thermally-Responsive Programmable Materials Based on Carbon Nanotube-Hydrogel Polymer Composites. *Nano Letters* **2011**, *11*, 3239–3244, doi:10.1021/nl201503e.

48. Kim, D.; Lee, H. S.; Yoon, J. Highly bendable bilayer-type photo-actuators comprising of reduced graphene oxide dispersed in hydrogels. *Scientific Reports* **2016**, *6*, doi:10.1038/srep20921.
49. Wang, E.; Desai, M. S.; Lee, S.-W. Light-Controlled Graphene-Elastin Composite Hydrogel Actuators. *Nano Letters* **2013**, *13*, 2826–2830, doi:10.1021/nl401088b.
50. Jeon, S.-J.; Hayward, R. C. Reconfigurable Microscale Frameworks from Concatenated Helices with Controlled Chirality. *Advanced Materials* **2017**, *29*, 1606111, doi:10.1002/adma.201606111.
51. Jeong, J.; Cho, Y.; Lee, S. Y.; Gong, X.; Kamien, R. D.; Yang, S.; Yodh, A. G. Topography-guided buckling of swollen polymer bilayer films into three-dimensional structures. *Soft Matter* **2017**, *13*, 956–962, doi:10.1039/C6SM02299E.
52. Wang, Z. J.; Zhu, C. N.; Hong, W.; Wu, Z. L.; Zheng, Q. Programmed planar-to-helical shape transformations of composite hydrogels with bioinspired layered fibrous structures. *Journal of Materials Chemistry B* **2016**, *4*, 7075–7079, doi:10.1039/C6TB02178F.
53. Wie, J. J.; Lee, K. M.; White, T. J. Thermally and Optically Fixable Shape Memory in Azobenzene-Functionalized Glassy Liquid Crystalline Polymer Networks. *Molecular Crystals and Liquid Crystals* **2014**, *596*, 113–121, doi:10.1080/15421406.2014.918336.
54. White, T. J.; Broer, D. J. Programmable and adaptive mechanics with liquid crystal polymer networks and elastomers. *Nature Materials* **2015**, *14*, 1087–1098, doi:10.1038/nmat4433.
55. Gu, W.; Wei, J.; Yu, Y. Thermo- and photo-driven soft actuators based on crosslinked liquid crystalline polymers. *Chinese Physics B* **2016**, *25*, 096103, doi:10.1088/1674-1056/25/9/096103.
56. Kularatne, R. S.; Kim, H.; Boothby, J. M.; Ware, T. H. Liquid crystal elastomer actuators: Synthesis, alignment, and applications. *Journal of Polymer Science Part B: Polymer Physics* **2017**, *55*, 395–411, doi:10.1002/polb.24287.
57. Ohm, C.; Brehmer, M.; Zentel, R. Liquid Crystalline Elastomers as Actuators and Sensors. *Advanced Materials* **2010**, *22*, 3366–3387, doi:10.1002/adma.200904059.
58. Ionov, L. Polymeric Actuators. *Langmuir* **2015**, *31*, 5015–5024, doi:10.1021/la503407z.
59. Chen, Z.; Huang, G.; Trase, I.; Han, X.; Mei, Y. Mechanical Self-Assembly of a Strain-Engineered Flexible Layer: Wrinkling, Rolling, and Twisting. *Physical Review Applied* **2016**, *5*, doi:10.1103/PhysRevApplied.5.017001.
60. de Haan, L. T.; Schenning, A. P. H. J.; Broer, D. J. Programmed morphing of liquid crystal networks. *Polymer* **2014**, *55*, 5885–5896, doi:10.1016/j.polymer.2014.08.023.
61. Meng, H.; Li, G. Reversible switching transitions of stimuli-responsive shape changing polymers. *Journal of Materials Chemistry A* **2013**, *1*, 7838, doi:10.1039/c3ta10716g.
62. Meng, H.; Mohamadian, H.; Stubblefield, M.; Jerro, D.; Ibekwe, S.; Pang, S.-S.; Li, G. Various shape memory effects of stimuli-responsive shape memory polymers. *Smart Materials and Structures* **2013**, *22*, 093001, doi:10.1088/0964-1726/22/9/093001.

63. Oliver, K.; Seddon, A.; Trask, R. S. Morphing in nature and beyond: a review of natural and synthetic shape-changing materials and mechanisms. *Journal of Materials Science* **2016**, *51*, 10663–10689, doi:10.1007/s10853-016-0295-8.
64. Wang, L.; Li, Q. Stimuli-Directing Self-Organized 3D Liquid-Crystalline Nanostructures: From Materials Design to Photonic Applications. *Advanced Functional Materials* **2016**, *26*, 10–28, doi:10.1002/adfm.201502071.
65. Yang, Y.; Zhang, Y.; Wei, Z. Supramolecular Helices: Chirality Transfer from Conjugated Molecules to Structures. *Advanced Materials* **2013**, *25*, 6039–6049, doi:10.1002/adma.201302448.
66. Urayama, K. Switching shapes of nematic elastomers with various director configurations. *Reactive and Functional Polymers* **2013**, *73*, 885–890, doi:10.1016/j.reactfunctpolym.2012.10.008.
67. Sawa, Y.; Urayama, K.; Takigawa, T.; Gimenez-Pinto, V.; Mbanga, B. L.; Ye, F.; Selinger, J. V.; Selinger, R. L. B. Shape and chirality transitions in off-axis twist nematic elastomer ribbons. *Physical Review E* **2013**, *88*, doi:10.1103/PhysRevE.88.022502.
68. Mol, G. N.; Harris, K. D.; Bastiaansen, C. W. M.; Broer, D. J. Thermo-Mechanical Responses of Liquid-Crystal Networks with a Splayed Molecular Organization. *Advanced Functional Materials* **2005**, *15*, 1155–1159, doi:10.1002/adfm.200400503.
69. Tomassetti, G.; Varano, V. Capturing the helical to spiral transitions in thin ribbons of nematic elastomers. *Meccanica* **2017**, *52*, 3431–3441, doi:10.1007/s11012-017-0631-3.
70. Teresi, L.; Varano, V. Modeling helicoid to spiral-ribbon transitions of twist-nematic elastomers. *Soft Matter* **2013**, *9*, 3081, doi:10.1039/c3sm27491h.
71. Lee, K. M.; Bunning, T. J.; White, T. J. Autonomous, Hands-Free Shape Memory in Glassy, Liquid Crystalline Polymer Networks. *Advanced Materials* **2012**, *24*, 2839–2843, doi:10.1002/adma.201200374.
72. Liu, L.; Geng, B.; Sayed, S. M.; Lin, B.-P.; Keller, P.; Zhang, X.-Q.; Sun, Y.; Yang, H. Single-layer dual-phase nematic elastomer films with bending, accordion-folding, curling and buckling motions. *Chemical Communications* **2017**, *53*, 1844–1847, doi:10.1039/C6CC08976C.
73. Wie, J. J.; Lee, K. M.; Ware, T. H.; White, T. J. Twists and Turns in Glassy, Liquid Crystalline Polymer Networks. *Macromolecules* **2015**, *48*, 1087–1092, doi:10.1021/ma502563q.
74. Agrawal, A.; Yun, T.; Pesek, S. L.; Chapman, W. G.; Verduzco, R. Shape-responsive liquid crystal elastomer bilayers. *Soft Matter* **2014**, *10*, 1411–1415, doi:10.1039/C3SM51654G.
75. Boothby, J. M.; Ware, T. H. Dual-responsive, shape-switching bilayers enabled by liquid crystal elastomers. *Soft Matter* **2017**, *13*, 4349–4356, doi:10.1039/C7SM00541E.
76. Priimagi, A.; Barrett, C. J.; Shishido, A. Recent twists in photoactuation and photoalignment control. *J. Mater. Chem. C* **2014**, *2*, 7155–7162, doi:10.1039/C4TC01236D.

77. Iamsaard, S.; Villemin, E.; Lancia, F.; Aβhoff, S.-J.; Fletcher, S. P.; Katsonis, N. Preparation of biomimetic photoresponsive polymer springs. *Nature Protocols* **2016**, *11*, 1788–1797, doi:10.1038/nprot.2016.087.
78. Harris, K. D.; Cuypers, R.; Scheibe, P.; van Oosten, C. L.; Bastiaansen, C. W. M.; Lub, J.; Broer, D. J. Large amplitude light-induced motion in high elastic modulus polymer actuators. *Journal of Materials Chemistry* **2005**, *15*, 5043, doi:10.1039/b512655j.
79. Iamsaard, S.; Aßhoff, S. J.; Matt, B.; Kudernac, T.; Cornelissen, J. J. L. M.; Fletcher, S. P.; Katsonis, N. Conversion of light into macroscopic helical motion. *Nature Chemistry* **2014**, *6*, 229–235, doi:10.1038/nchem.1859.
80. Wang, M.; Lin, B.-P.; Yang, H. A plant tendril mimic soft actuator with phototunable bending and chiral twisting motion modes. *Nature Communications* **2016**, *7*, 13981, doi:10.1038/ncomms13981.
81. Boothby, J. M.; Kim, H.; Ware, T. H. Shape changes in chemoresponsive liquid crystal elastomers. *Sensors and Actuators B: Chemical* **2017**, *240*, 511–518, doi:10.1016/j.snb.2016.09.004.
82. de Haan, L. T.; Verjans, J. M. N.; Broer, D. J.; Bastiaansen, C. W. M.; Schenning, A. P. H. J. Humidity-Responsive Liquid Crystalline Polymer Actuators with an Asymmetry in the Molecular Trigger That Bend, Fold, and Curl. *Journal of the American Chemical Society* **2014**, *136*, 10585–10588, doi:10.1021/ja505475x.
83. Kamal, T.; Park, S. Shape-Responsive Actuator from a Single Layer of a Liquid-Crystal Polymer. *ACS Applied Materials & Interfaces* **2014**, *6*, 18048–18054, doi:10.1021/am504910h.
84. Kaiser, A.; Winkler, M.; Krause, S.; Finkelmann, H.; Schmidt, A. M. Magnetoactive liquid crystal elastomer nanocomposites. *J. Mater. Chem.* **2009**, *19*, 538–543, doi:10.1039/B813120C.
85. Winkler, M.; Kaiser, A.; Krause, S.; Finkelmann, H.; Schmidt, A. M. Liquid Crystal Elastomers with Magnetic Actuation. *Macromolecular Symposia* **2010**, *291–292*, 186–192, doi:10.1002/masy.201050522.
86. Zhou, Y.; Sharma, N.; Deshmukh, P.; Lakhman, R. K.; Jain, M.; Kasi, R. M. Hierarchically Structured Free-Standing Hydrogels with Liquid Crystalline Domains and Magnetic Nanoparticles as Dual Physical Cross-Linkers. *Journal of the American Chemical Society* **2012**, *134*, 1630–1641, doi:10.1021/ja208349x.
87. Huang, W. M.; Ding, Z.; Wang, C. C.; Wei, J.; Zhao, Y.; Purnawali, H. Shape memory materials. **2010**, *13*, 8.
88. Mendez, J.; Annamalai, P. K.; Eichhorn, S. J.; Rusli, R.; Rowan, S. J.; Foster, E. J.; Weder, C. Bioinspired Mechanically Adaptive Polymer Nanocomposites with Water-Activated Shape-Memory Effect. *Macromolecules* **2011**, *44*, 6827–6835, doi:10.1021/ma201502k.
89. Montero de Espinosa, L.; Meesorn, W.; Moatsou, D.; Weder, C. Bioinspired Polymer Systems with Stimuli-Responsive Mechanical Properties. *Chemical Reviews* **2017**, *117*, 12851–12892, doi:10.1021/acs.chemrev.7b00168.

90. Janbaz, S.; Hedayati, R.; Zadpoor, A. A. Programming the shape-shifting of flat soft matter: from self-rolling/self-twisting materials to self-folding origami. *Materials Horizons* **2016**, *3*, 536–547, doi:10.1039/C6MH00195E.
91. Lendlein, A.; Kelch, S. Shape-Memory Polymers. *Angewandte Chemie International Edition* **2002**, *41*, 2034, doi:10.1002/1521-3773(20020617)41:12<2034::AID-ANIE2034>3.0.CO;2-M.
92. Robertson, J. M.; Torbati, A. H.; Rodriguez, E. D.; Mao, Y.; Baker, R. M.; Qi, H. J.; Mather, P. T. Mechanically programmed shape change in laminated elastomeric composites. *Soft Matter* **2015**, *11*, 5754–5764, doi:10.1039/C5SM01004G.
93. Gerbode, S. J.; Puzey, J. R.; McCormick, A. G.; Mahadevan, L. How the Cucumber Tendril Coils and Overwinds. *Science* **2012**, *337*, 1087–1091, doi:10.1126/science.1223304.
94. Liu, J.; Huang, J.; Su, T.; Bertoldi, K.; Clarke, D. R. Structural Transition from Helices to Hemihelices. *PLoS ONE* **2014**, *9*, e93183, doi:10.1371/journal.pone.0093183.
95. Silva, P. E. S.; Trigueiros, J. L.; Trindade, A. C.; Simoes, R.; Dias, R. G.; Godinho, M. H.; de Abreu, F. V. Perversions with a twist. *Scientific Reports* **2016**, *6*, doi:10.1038/srep23413.
96. Tomsett, M.; Maffucci, I.; Le Bailly, B. A. F.; Byrne, L.; Bijvoets, S. M.; Lizio, M. G.; Raftery, J.; Butts, C. P.; Webb, S. J.; Contini, A.; Clayden, J. A tendril perversion in a helical oligomer: trapping and characterizing a mobile screw-sense reversal. *Chemical Science* **2017**, *8*, 3007–3018, doi:10.1039/C6SC05474A.
97. Huang, J.; Liu, J.; Kroll, B.; Bertoldi, K.; Clarke, D. R. Spontaneous and deterministic three-dimensional curling of pre-strained elastomeric bi-strips. *Soft Matter* **2012**, *8*, 6291, doi:10.1039/c2sm25278c.
98. Kim, T.; Zhu, L.; Mueller, L. J.; Bardeen, C. J. Mechanism of Photoinduced Bending and Twisting in Crystalline Microneedles and Microribbons Composed of 9-Methylanthracene. *Journal of the American Chemical Society* **2014**, *136*, 6617–6625, doi:10.1021/ja412216z.
99. Chen, Z. Geometric nonlinearity and mechanical anisotropy in strained helical nanoribbons. *Nanoscale* **2014**, *6*, 9443–9447, doi:10.1039/C4NR00336E.
100. Abraham, Y.; Tamburu, C.; Klein, E.; Dunlop, J. W. C.; Fratzl, P.; Raviv, U.; Elbaum, R. Tilted cellulose arrangement as a novel mechanism for hygroscopic coiling in the stork's bill awn. *Journal of The Royal Society Interface* **2012**, *9*, 640–647, doi:10.1098/rsif.2011.0395.
101. Rong, Q.-Q.; Cui, Y.-H.; Shimada, T.; Wang, J.-S.; Kitamura, T. Self-shaping of bioinspired chiral composites. *Acta Mechanica Sinica* **2014**, *30*, 533–539, doi:10.1007/s10409-014-0012-2.
102. Lima, M. D.; Li, N.; Jung de Andrade, M.; Fang, S.; Oh, J.; Spinks, G. M.; Kozlov, M. E.; Haines, C. S.; Suh, D.; Foroughi, J.; Kim, S. J.; Chen, Y.; Ware, T.; Shin, M. K.; Machado, L. D.; Fonseca, A. F.; Madden, J. D. W.; Voit, W. E.; Galvao, D. S.; Baughman, R. H. Electrically, Chemically, and Photonically Powered Torsional and Tensile Actuation of Hybrid Carbon Nanotube Yarn Muscles. *Science* **2012**, *338*, 928–932, doi:10.1126/science.1226762.

967 103. Kim, S. H.; Kwon, C. H.; Park, K.; Mun, T. J.; Lepró, X.; Baughman, R. H.; Spinks,
968 G. M.; Kim, S. J. Bio-inspired, Moisture-Powered Hybrid Carbon Nanotube Yarn
969 Muscles. *Scientific Reports* **2016**, *6*, doi:10.1038/srep23016.
970 104. Deng, J.; Xu, Y.; He, S.; Chen, P.; Bao, L.; Hu, Y.; Wang, B.; Sun, X.; Peng, H.
971 Preparation of biomimetic hierarchically helical fiber actuators from carbon nanotubes.
972 *Nature Protocols* **2017**, *12*, 1349–1358, doi:10.1038/nprot.2017.038.
973 105. Chen, P.; He, S.; Xu, Y.; Sun, X.; Peng, H. Electromechanical Actuator Ribbons
974 Driven by Electrically Conducting Spring-Like Fibers. *Advanced Materials* **2015**, *27*,
975 4982–4988, doi:10.1002/adma.201501731.
976 106. Guo, Q.; Dai, E.; Han, X.; Xie, S.; Chao, E., and Chen, Z. Fast nastic motion of
977 plants and bio-inspired structures, *Journal of the Royal Society Interface* **2015**, 12: 20150598,
978 doi: 10.1098/rsif.2015.0598.
979